A Novel Mineralizing film Induces Biomimetic Mineralization

Zhe Wang
zhe jiang da xue: Zhejiang University
Zihuai Zhou
zhe jiang da xue: Zhejiang University
Jiayan Fan
zhe jiang da xue: Zhejiang University
Leiqing Zhang
zhe jiang da xue: Zhejiang University
Zhixin Zhang
zhe jiang da xue: Zhejiang University
Zhifang Wu
zhe jiang da xue: Zhejiang University
Ying Shi
zhe jiang da xue: Zhejiang University
Haiyan Zheng
zhe jiang da xue: Zhejiang University
Zhengyi Zhang
zhe jiang da xue: Zhejiang University
Ruikang Tang
zhe jiang da xue: Zhejiang University
Baiping Fu (fbp@zju.edu.cn)
zhe jiang da xue: Zhejiang University

Research Article

Keywords: Caries, Hydroxypropylmethylcellulose, film, biomimetic mineralization, dentin, collagen

Posted Date: August 16th, 2021

DOI: https://doi.org/10.21203/rs.3.rs-812325/v1

A Novel Mineralizing film Induces Biomimetic Mineralization

*Zhe Wang,[1‡] Zihuai Zhou,[1‡] Jiayan Fan,[1] Leiqing Zhang,[1] Zhixin Zhang,[1] Zhifang Wu,[1] Ying Shi,[1] Haiyan Zheng,[1] Zhengyi Zhang,[1] Ruikang Tang,[2] and Baiping Fu,[1]**

Abstract

Demineralization of tooth hard tissues leads to dental caries, which causes health problem and economic burden throughout the world. Biomimetic mineralization strategy is expected to reverse initial dental caries. Commercially available mineralizing anti-carious products lead to indefinite clinical results because they could not continuously replenish calcium and phosphate resources. Herein, we prepared a novel mineralizing film (NMF) consisting of hydroxypropylmethylcellulose (HPMC) and polyaspartic acid-stabilized amorphous calcium phosphate (PAsp-ACP) nanoparticles. HPMC containing multiple hydroxyls is a gel-forming material that could be either desiccated to be a dry film or gradually changed into gel in moist milieu. The HPMC was, for the first time, used as a carrier of PAsp-ACP nanoparticles for delivering biomimetic mineralization in moist milieu. Our results indicated the hydroxyls and methoxyls of HPMC could assist the stability of PAsp-ACP nanoparticles and maintain their bioactivity of mineralization. The results further demonstrated that the NMF bioinspired the early mineralization of demineralized dentin at 24 hrs and the heavy mineralization of the whole demineralized dentin (3-4 μm) at 72-96 hrs without any cytotoxicity and mucosa irritation. Therefore, the NMF might be promising mineralizing strategy for preventive dentistry with efficient mineralization capability.

Keywords

Caries, Hydroxypropylmethylcellulose, film, biomimetic mineralization, dentin, collagen

Background

Dental caries is one of the most prevalent and consequential diseases in the world [1]. The latest data on the global burden of diseases (March 2020) show that over 3.5 billion people suffer from dental caries, which remains a neglected global health issue [2]. Additionally, dental caries is a predictably increasing social and economic burden [3]. We should therefore take measures to prevent dental caries.

Recently, scientists have adopted biomimetic mineralization as a minimally invasive method for treating initial caries [4]. Most detectable caries not only demineralizes enamel but also dentin. Dentin consists of a mineralized collagen matrix. Biomimetic mineralization is an organics-mediated process involving the formation of heterogeneous crystal nuclei [5]. Most of the current biomimetic mineralization studies are based on the polymer-induced liquid-precursor (PILP) theory [6]. Polymers play an essential role in the transformation of precursors (amorphous calcium phosphate, ACP) into hydroxyapatite (HAp) during biomimetic mineralization [7]. The ACP nanoparticles are believed to be crucial precursors in biomimetic mineralization [8]. However, in aqueous solutions, the ACP nanoparticles are easily converted into crystalline phases [9]. Only when ACP nanoparticles are kept under dry conditions or stabilized by polyelectrolytes, such as

polyaspartic acid (PAsp) or polyacrylic acid (PAA), they can maintain their mineralization activity. In addition, some polymers, such as poly(amide amine) (PAMAM) and polyethylene glycol hydrogels are also used to stabilize the ACP nanoparticles [10,11]. Based on the PILP theory, commercially available contemporary anti-carious materials have been developed to deliver mimetic mineralization in liquid (mouth rinse) and paste (toothpaste) [12]. However, their dentin remineralization efficacy is not as good as expected because they do not continuously release calcium and phosphate resources for biomimetic mineralization [13]. Moreover, mesoporous silica have been used as a carrier to deliver the ACP nanoparticles [14]. Our previous studies demonstrated that acidic, self-etching adhesives can be loaded with PAA-ACP or PAsp-Si-ACP nanoparticles to implement the biomimetic mineralization of demineralized dentin [15,16].

Hydroxypropylmethylcellulose (HPMC) is a nontoxic polymer that contains a large number of hydroxyl, methyl and methoxy anion groups [17]. It has been widely used as a drug carrier in pharmaceutical applications because it can be used as a film-forming material [18]. Once the dry HPMC film contacts water, its polymer chains relax, and its volume expands during gel formation. Loaded particles can be released [19]. To date, it has not yet been investigated how the HPMC can be used as a carrier for ACP nanoparticles to deliver biomimetic mineralization. Therefore, in this work, we proposed a novel, film-assisted biomimetic mineralization strategy. We demonstrated that the NMF could deliver the biomimetic mineralization without any cytotoxicity and mucosa irritation. An early mineralization of demineralized dentin occurred at 24 hrs, and a heavy

mineralization of the whole demineralized dentin (3-4 μm) took place at 72-96 hrs. The Cryo-TEM images indicate the NMF could release the ACP nanoparticles at early stage, maintain their bioactivity in an amorphous phase at 6 hrs and they gradually transformed into HAp at 8 hrs when exposed to artificial saliva at 37 °C. The HPMC was, for the first time, used as a carrier of the ACP nanoparticles for delivering biomimetic mineralization via hydroxyls and methoxyls of the HPMC in synergism with polyelectrolytes. Hence, the NMF might be promising mineralizing strategy for preventive dentistry with an efficient mineralization capability.

Materials and methods

Synthesis and characterization of PAsp-stabilized ACP nanoparticles (PAsp-ACP nanoparticles)

PAsp-ACP nanoparticles were synthesized by mixing equal volumes (25 mL) of 6 mM Na_2HPO_4 and 10 mM $CaCl_2$/480 μg mL^{-1} PAsp, and stirring for 10 min at room temperature. During synthesis process, the pH of the solution was gradually adjusted to 9.5 ± 0.1 by titrating 5 mol NaOH. The precipitates (PAsp-ACP nanoparticles) were collected by centrifugation (18000 rpm, 5 min, F0650, Beckman Allegra64R, USA), and subsequently washed with absolute ethanol thrice. Subsequently, the PAsp-ACP nanoparticles were dried in a vacuum drying oven at 30 °C overnight before they were analyzed by scanning electron microscopy (SEM, HITACHI，SU8010, Tokyo, Japan), transmission electron microscopy (TEM, JEM-1230, JEOL, Tokyo, Japan), powder X-ray diffractometry (XRD, Rigaku D/MAX-2550 pc, Japan) and Fourier transform infrared spectroscopy (FTIR, Spectrum 400, Perkin-Elmer, USA)

Preparation and characterization of mineralizing film

A mineralizing film was prepared as follows: HPMC (0.24 g) powders were immersed in 1.5 mL of 70% alcohol for 12 hrs in order to obtain HPMC gel. Subsequently, 0.24 g of PAsp-ACP nanoparticles, and 2 mL of 70% alcohol were added to HPMC gel, and then the mixtures were stirred magnetically at room temperature for 5 min. Afterward, 2 mm thickness of the mixture were prepared on a glass slide and dried under an infrared light for 2 hrs to form a big piece of mineralizing film with a size of 48 mm x 25 mm. Finally, the film was cut into small pieces of 5 mm x 5 mm and stored in a desiccator. The mineralizing films were analyzed by SEM, TEM, FTIR and XRD. The pure HPMC film was prepared as the same as the aforementioned procedure, and also analyzed by FTIR and XRD.

ICP-AES measurements

A big piece of the aforementioned mineralizing film was stored in artificial saliva for 24 hrs. One hundred μL of the supernatant was retrieved at each time point (4, 8, 12, 16, 20, 24 hrs) and diluted to 100 mL with deionized water. Afterward, the concentrations of Ca and P elements were measured by inductively coupled plasma-atomic emission spectrometer (ICP-AES, Thermo iCAP-6300, USA). The measurements were performed in triplicate.

Phase transformation of Mineralizing film in artificial saliva—FTIR analysis

A big piece of mineralizing film was immersed in 60 mL of artificial saliva in a 100% humidity chamber at 37 °C for 48 hrs. One mL of the mixture was respectively retrieved at each time point (6, 8, 10, 12, 24, 48 hrs). The solid materials from the mixture were collected by centrifugation, washed with absolute ethanol thrice, and dried overnight in a vacuum oven at 30°C before they

were analyzed by FTIR. A piece of pure HPMC film was also analyzed by FTIR. The splitting function （SF）proposed by Posner was used to determine the phase transformation of mineralizing film in artificial saliva [20].

Phase transformation of Mineralizing film in artificial saliva—Cryo-TEM analysis

The phase transformation of ACP nanoparticles in HPMC in artificial saliva was each analyzed at the time point (0, 6, 8, 12，24 hrs) by cryo-transmission electron microscopy (Cryo-TEM, Talos F200C, FEI, USA). The samples for Cryo-TEM were described in the ESI†.

Biocompatibility test—Cytotoxicity test in vitro

The cytotoxicity of mineralizing film was assessed by Cell Counting Kit-8 (CCK-8) assay (Beyotime, Shanghai, China). The mineralizing films at different concentrations (0.1, 0.2, 0.5, 1, 2, 4, 8, 16 mg mL^{-1}) were incubated at 37 °C in Duibecco's modified Eagle's medium (DMEM, Gibco, USA) for 24 hrs to obtain leach solutions, in which 10 % of fetal bovine serum (FBS, Gibco, USA) was supplemented. Afterward, the L929 cell (Cell Collection, Shanghai, China) was planted into 96-well plates with 10000 cells each well. They were incubated for 24 hrs to allow cell attachment. Then, the attached cells were incubated with 5 % of CO_2 and 95% relative humidity in each well with the different leach solutions for 24 hrs at 37°C. Afterward, each well was added with 10 μL CCK-8 and the attached cells were incubated for another 2-3 hrs. The measurements were performed six times at 450 nm absorbance using a microplate reader (Bio Tek Eon, USA).

Biocompatibility test—Oral mucosa irritation tests in vivo

The protocol design was based on the Stimulation and Skin Allergy Test, Appendix B.3 Oral Mucosal Stimulation Test (ISO 10993-10, 2010) [21]. Six male golden hamsters with a weigh range of 110-130 g were purchased from Beijing Weitong Lihua experimental animal company (an animal production license: SCXK (Beijing) 2016-0011). After acclimatization for 1 week, the golden hamsters on the 8th day were anesthetized by intraperitoneally injecting with 30 g L^{-1}, sodium pentobarbital (0.002mLg^{-1}). After 0.2 g mineralizing film was immersed in 1 mL of 0.9% NaCl and 1 mL of cottonseed oil for 24 hrs, a cotton ball in a diameter of approximately 0.40-0.45 cm was soaked with 50 μL of the mineralizing film polar (0.9% NaCL) and non-polar (cottonseed oil) extracts, and subsequently placed in the left and right cheek pouch of the golden hamster. Oral mucosa irritation test was performed 4 times, 10 min each time, at 1 hr of interval. Macro- and micro-scopic histological evaluations of the irritated buccal mucosa were performed. The preparation of buccal mucosa samples for microscopic histological evaluation and its grading system were described in the ESI†.

Biomimetic mineralization of demineralized dentin—In vitro experiment

The preparation of demineralized dentin disks and the samples for TEM were described in the ESI†. The demineralized dentin disks (N=36) were randomly divided into three groups (n=12): The demineralized dentin disk samples were not covered with anything serving as control. The demineralized dentin disk samples were covered either with pure HPMC films or with mineralizing films. Each sample was placed in 1 mL of artificial saliva in a well of 48-well plates, and incubated in a 100% humidity chamber at 37 °C. HPMC films, mineralizing films and artificial saliva were changed daily. Four samples were retrieved after incubation for 1, 2, 3, and 4 d in preparation for ultrathin sections. Then, they were analyzed by TEM with SAED, high resolution TEM (HRTEM) and element mapping. The micro-mechanical property of the intact, de- and re-mineralized dentin

(4 d) in moist condition were determined by a Nanoindenter G200 (Agilent, USA) with a Berkovich diamond indenter. The sample preparations for indentation test were described in the ESI†. The measurement depth was set at 2500 nm for 10 s of a peak hold time and Poisson Ratio was set at 0.28. Five points were randomly chosen on each dentin disk surface.

Biomimetic mineralization of demineralized dentin—In vivo experiments

A total of 6 healthy, male New Zealand rabbits (Certificate number: SCXK (Zhe) 2017-0004) with 12 weeks of age and 2.1-2.5 Kg of weight were purchased (Hangzhou Yuhang Kelian Rabbit Industry Professional Cooperative, Hangzhou, China) in this study. Demineralized dentin was prepared as follows: Six rabbits were anesthetized with 10% chloral hydrate (0.4 mg/kg, Dopalen, Ceva Sante Animale, Libourne, France), and the labial enamel surfaces of the rabbits' maxillary and mandibular central incisors were completely removed to expose the dentin surfaces. Afterward, the exposed dentin surfaces were etched with 37% phosphoric acid gel for 15 s and thoroughly rinsed with water. The maxillary central incisors were used for biomimetic mineralization, and the mandibular central incisors served as blank control. (1) Control group: Demineralized dentin surfaces of the mandibular central incisors were directly exposed to the oral cavity without covering of any mineralized films. (2) Experimental group: Transparent custom trays were prepared in the ESI†. The demineralized dentin surfaces of the maxillary central incisors were covered with the mineralizing films and subsequently the central incisors were protected with the transparent splint, 8 hrs a day, 7 consecutive days. Finally, all the rabbits were sacrificed and the central incisors were obtained. The incisor samples were prepared into ultrathin sections in the ESI†, and examined by TEM with SAED.

Results and discussion

Characterization of the PAsp-ACP nanoparticles

PAsp-ACP nanoparticles were synthesized and incorporated into HPMC as a dry mineralizing film**.** Scanning electron microscopy (SEM) and transmission electron microscopy (TEM) micrographs show that the PAsp-ACP nanoparticles are spherical (Fig.1 a and b). The diameter of an individual nanoparticle is approximately 30-80 nm (Fig.1 a and b). The Fourier transform infrared spectroscopy (FTIR) spectrum of the nanoparticles shows characteristic PAsp-ACP peaks at 1050 cm^{-1} and 580 cm^{-1} (Fig.1 c) [22]. The X-ray diffraction (XRD) pattern for the nanoparticles indicates a broad peak at $2\theta=30°$ (Fig.1 d). Both the FTIR spectrum and XRD pattern indicate that the PAsp-ACP nanoparticles are amorphous [22,23]. According to previous studies, ACP nanoparticles are unstable in solution and easily transform into HAp [8]. As such, the clinical applications of ACP nanoparticles are limited. PAsp is a noncollagen protein (NCP) analog that plays an important role in stabilizing ACP, allowing it to enter collagen fibrils for mineralization [24]. Under dry conditions, PAsp-stabilized ACP nanoparticles can easily be kept in an amorphous phase [25].

Characterization of the novel mineralizing film

The mineralizing film is very stable under dry conditions and promising for clinical applications. SEM images show that the PAsp-ACP nanoparticles are uniformly distributed in the mineralizing film (Fig.1 e). TEM images demonstrate that the PAsp-ACP nanoparticles in the mineralizing film are 30-80 nm in diameter and amorphous (selected area electron diffraction (SAED) inset, Fig.1 f). A characteristic FTIR peak is observed at 580 cm^{-1} and is not split, indicating that the PAsp-ACP nanoparticles are amorphous in the mineralizing film (Fig.1 g, blue line). The absorption peaks between 1300 cm^{-1} and 1750 cm^{-1} are attributed to tightly bound water (10–20%) in the ACP

nanoparticles (Fig.1 g, red line) [25]. The characteristic HPMC peaks are mainly those observed at 1065 cm^{-1}, attributed to C-O-C asymmetric stretching vibrations, and1119 cm^{-1}, attributed to C-O stretching vibrations [26]. The absorption peaks at 872 cm^{-1} and 1420 cm^{-1} correspond to the characteristic peaks of CO_3^{2-} (Fig.1 g, black line). The XRD pattern exhibits a broad peak at 2θ=30°, indicating that the ACP nanoparticles are amorphous (Fig.1 h) [22,23]. Thus, HPMC can be used as a carrier to deliver ACP precursors and promote biomimetic mineralization; HPMC can not only maintain ACP precursor bioactivity under dry conditions but can also be easily prepared and applied due to its interchangeable properties (from solid to gel and from gel to solid).

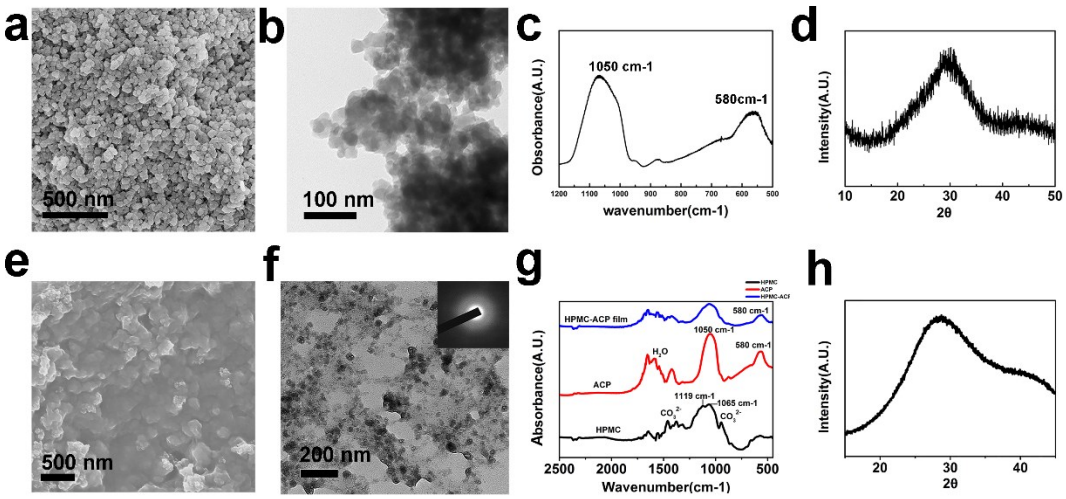

Fig.1 Characterization of the PAsp-ACP nanoparticles and the novel mineralizing film. a) SEM image showing that the spherical PAsp-ACP nanoparticles are clustered together. b) TEM image showing that the PAsp-ACP nanoparticles have diameters of approximately 30-80 nm. c) FTIR spectrum of the PAsp-ACP nanoparticles showing two characteristic PO_4^{3-} absorption peaks at 1050 cm^{-1} and 580 cm^{-1}. d) XRD pattern exhibiting a broad peak at 2θ=30°. e) SEM image showing that the PAsp-ACP nanoparticles are homogeneously distributed in the mineralizing film. f) TEM image showing that the spherical PAsp-ACP nanoparticles are dispersed in HPMC, and

the SAED pattern (inset panel) indicates that the ACP nanoparticles are amorphous. g) FTIR spectrum showing that HPMC exhibits a typical C-O peak at 1065 cm^{-1}, a C-O-C peak at 1119 cm^{-1}, and CO_3^{2-} peaks at 872 cm^{-1} and 1420 cm^{-1}. The ACP nanoparticles exhibit characteristic PO_4^{3-} absorption peaks at 1050 cm^{-1} and 580 cm^{-1} as well as absorption peaks attributed to bound water at 1300 cm^{-1} and 1750 cm^{-1} (red line). The NFM exhibits peaks characteristic of both HPMC and the ACP nanoparticles (blue line). h) The XRD pattern displays a broad peak at $2\theta=30°$.

ICP-AES measurements in the novel mineralizing film

Dentin mineralization is based on calcium and phosphate resources [27]. Fig.2 a shows that the amount of Ca and P increased quickly within 4 hrs after the mineralizing film was incubated in artificial saliva at 37°C. Between 4 hrs and 24 hrs, Ca and P were steadily released from the mineralizing film (Fig.2 a). According to previous studies, biological, crystalline apatite formation is initiated with the heterogeneous nucleation of inorganic calcium phosphate on an organic extracellular matrix [28]. The concentrations of free Ca ions and ACP are the main factors for HAp nucleation [29]. Previous studies have shown that HPMC has a high swell ability and surface activity. It can carry and deliver soluble and insoluble drug particles [18]. The results of inductively coupled plasma atomic emission spectroscopy (ICP-AES) measurements confirm that the mineralizing film can release ACP nanoparticles. The Ca/P-releasing capability of the mineralizing film suggests that dentin remineralization is possible.

Phase transformations in the novel mineralizing film

Once the dry mineralizing films intake artificial saliva, they gradually form sticky gels. In addition, the ACP nanoparticles are released into the artificial saliva and gradually transform into HAp. The ACP nanoparticle phase transformation in the mineralizing film occurs after 8 hrs incubation in

artificial saliva (Fig.2 b). The nanoparticles are mostly transformed into HAp after 48 hrs, as demonstrated by the peak at 580 cm^{-1} splitting into two peaks at 560 cm^{-1} and 600 cm^{-1} (Fig.2 b) and the value of the splitting function (SF) being close to 1; the SF evaluates the degree of ACP nanoparticle crystallization, with 0 representing noncrystallization and 1 representing complete crystallization (Fig.2 c, d) [30]. The hydroxyl and carbonyl groups of HPMC can attract calcium ions and delay the crystallization of ACP. This might retard the release of calcium ions from HPMC gels since pure PAsp-ACP nanoparticles in artificial saliva start to transform into HAp within 2~3 hrs (Fig.S1). Moreover, ACP nanoparticles are liquid-like, and HPMC can provide hydrophobic microdomains for hydrophilic particles to facilitate drug release [31]. This indicates that HPMC is not only a good carrier for ACP precursors but can also stabilize ACP nanoparticles. Therefore, HPMC and PAsp might have a synergistic stabilizing effect on ACP nanoparticles. The mineralizing film allows the ACP nanoparticles enough time to enter and mineralize dentin collagen fibrils.

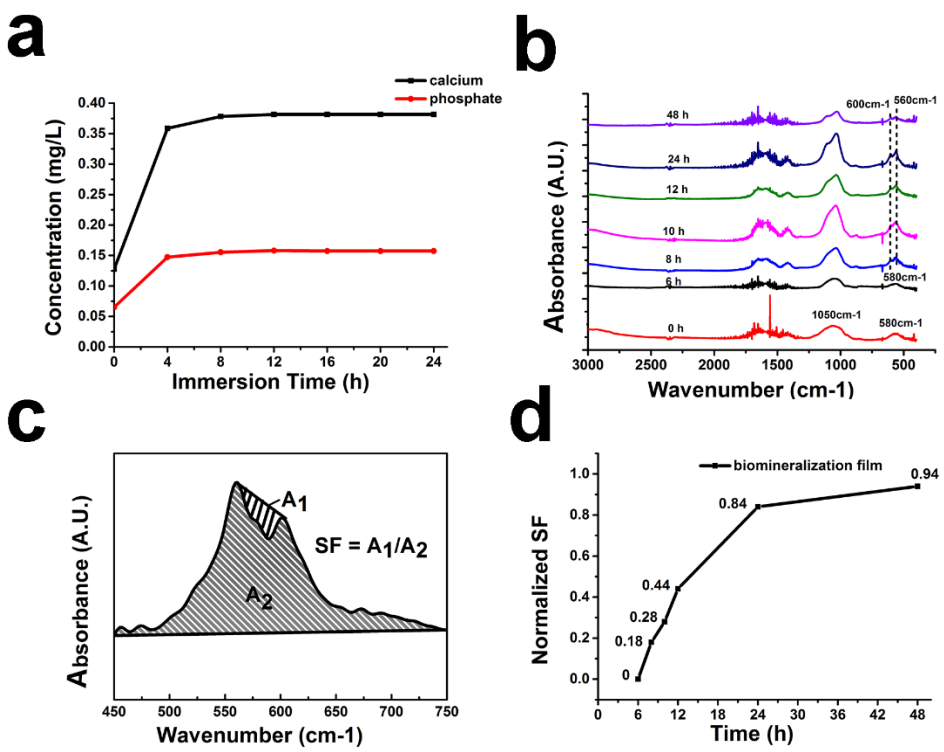

Fig.2 Ca and P release and phase transformations. a) Release kinetics for calcium (black line) and phosphate (red line) ions from the mineralizing film over 24 hrs. b) FTIR spectra of the mineralizing film showing a peak at 580 cm^{-1} at 6 hrs and two peaks at 560 cm^{-1} and 600 cm^{-1} at 8, 10, 12, 24, and 48 hrs. c) SF scheme. A1 indicates the valley area between the two peaks at 600 cm^{-1} and 560 cm^{-1}. A2 indicates the area between the baseline and the spectral curve ranging from 450 cm^{-1} to 750 cm^{-1}. SF: A1/A2 = 0 (noncrystallization) to 1 (complete crystallization). d) Kinetics of the ACP to HAp phase transformation. The SF is 0, 0.18, 0.28, 0.44, 0.84, and 0.94 at 0, 6, 10, 12, 24 and 48 hrs, respectively.

Cryo-TEM images indicate that the spherical ACP nanoparticles with diameters of approximately 30-80 nm remain amorphous within the first 6 hrs after the mineralizing film is incubated in artificial saliva (Fig.3 a, b, f, g). The nanoparticles become smaller, and adjacent ACP nanoparticles begin to fuse; some of the nanoparticles are transformed into weakly crystallized

HAp at 8 hrs (Fig.3 c, h). The reduced ACP nanoparticle size might result from dehydration during crystallization processes. The ACP nanoparticles start to transform into needle-like HAp with continuous 002, 211, and 004 diffraction rings after 12 hrs incubation (Fig.3 d, i) and are mostly observed as HAp at 24 hrs (Fig.3 i, j).

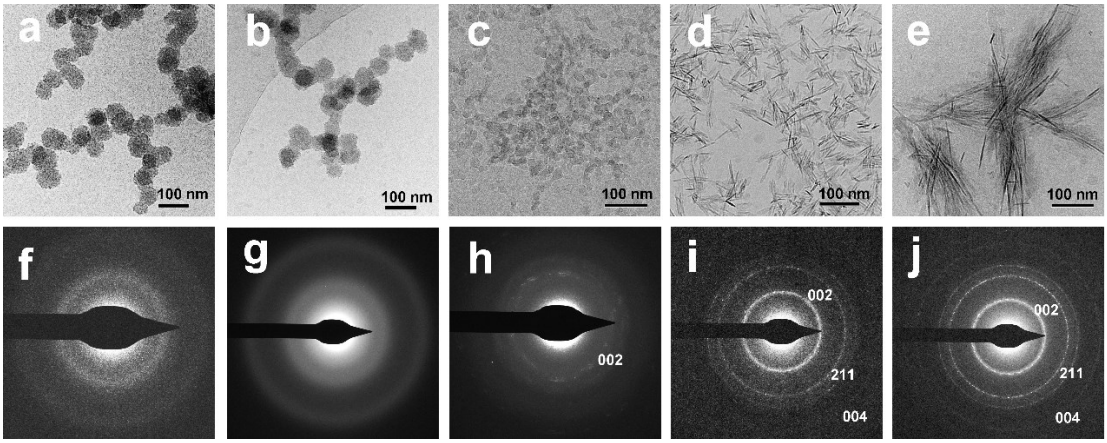

Fig.3 Cryo-TEM images of the mineralizing film and its SAED pattern at 0 hrs (panels a, f), 6 hrs (panels b, g), 8 hrs (panels c, h), 12 hrs (panels d, i) and 24 hrs (panels e, j) in artificial saliva. a) and b) The spherical ACP nanoparticles in the mineralizing film are approximately 30-80 nm in diameter and stable in artificial saliva over 6 hrs. c) The ACP nanoparticles decreased in size and fused at 8 hrs. d and e) Most of the ACP nanoparticles transformed into HAp at 12 and 24 hrs. f and g) SAED patterns indicate that the mineralizing film is amorphous at 0 (f) and 6 hrs (g); h） a discrete 002 diffraction ring is observed at 8 hrs, i and j) distinct 002, 211, and 004 diffraction rings are observed at 12 (i) and 24 hrs (j).

Taken together, the ICP data, FTIR spectra, SF data and Cryo-TEM images indicate that the mineralizing film does not only provide calcium and phosphate sources but also transforms into HAp when exposed to artificial saliva at 37 °C over reasonable application times (6-8 hrs). This

implies that the mineralizing film could be conveniently used for dentin mineralization over 6~8 hrs during sleep [32].

In vitro cytotoxicity tests of the novel mineralizing film

Based on cytotoxicity tests using L929 cells, which were performed with a CCK-8 assay (Fig.4 a), the mineralizing film possesses excellent biocompatibility even at a high concentration (16 mg mL^{-1}); this indicates that the mineralizing film could be used for biomedical applications. The results of the cytotoxicity tests performed in this study are consistent with the results of previous studies involving ACP nanoparticle-containing materials [33,34].

Oral mucosa irritation tests of the novel mineralizing film

Mineralizing films should not irritate the oral mucosa if they are expected to be used in clinical applications [35]. The results of histological examinations are summarized in Table 3 (Fig.S2), and representative histological images are shown in Fig.4. The mean score was 0 for all six groups (Fig.S2). No visible proliferation, alteration, degeneration or necrosis of epithelial cells was observed. No pathological changes, such as congestion, edema, inflammatory infiltration or necrosis under the mucosa, were detected (Fig.4 b-i). Therefore, the mineralizing film does not irritate the mucosa [35,36].

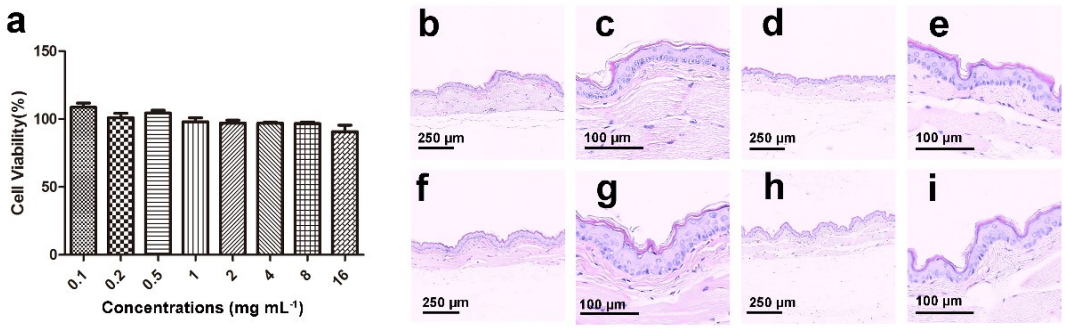

Fig.4 Cytotoxicity and oral mucosa irritation tests of the novel mineralizing film. a) Cell viability was assessed by a CCK-8 assay at different mineralizing film concentrations. The oral mucosas of golden hamster cheek pouches were treated with either a polar solvent (0.9% sodium chloride) (panels a, b) or a nonpolar solvent (cottonseed oil) (panels f, g) as control tests or with a polar extract (panels d, e) or a nonpolar extract of the mineralizing film (panels h, i). Panels f, g, h, and i are magnified views of panels b, c, d, and e. Epithelial cells did not proliferate or change. No degeneration, necrosis or leucocyte infiltration was observed. The vessels were not hyperemic. No edema or inflammatory cell infiltration were observed under the mucosa.

In vitro experiments of biomimetic mineralization of dentin

The mineralizing film was, for the first time, used as a carrier to achieve biomimetic mineralization of demineralized dentin. TEM images show that the remineralized dentin becomes darker and thicker over time. The SAED patterns (insets of Fig.5 e, f, g, h) reveal typical 002, 004 and 211 discrete rings. A thin, weakly crystallized remineralization layer of approximately 0.3-0.5 μm was detected at the bottom of the demineralized dentin after 24 hrs incubation (Fig.5 a, white dotted line). The thickness of the remineralization layer increased to approximately 1-1.2-μm after 48 hrs incubation, and the layer exhibited regular crystallinity (Fig.5 d, white dotted line). After 72 hrs incubation, the thickness of the layer increased to approximately 2-μm, and the layer exhibited good crystallinity but a low electron density (Fig.5 g, white dotted line). Complete remineralization was observed after 96 hrs incubation, and the final thickness of the layer was that of the demineralized dentin (Fig.5 j, white dotted line). The final electron density of the remineralized dentin was similar to that of the neighboring, intact dentin. The SAED patterns show characteristic HAp planes, such as the 002, 211, and 004 planes (insets in Fig.5 a, d, g, j, i).

Furthermore, the spherical ACP nanoparticles were attached to the surface of the demineralized dentin after 24 hrs incubation (Fig.5 c, white arrow). After 48 hrs incubation, some nanoparticles (Fig.5 f, black arrow) were present on the surface of the demineralized dentin, and some spherical ACP nanoparticles were observed in the middle of the demineralized dentin layer (Fig.5 e, f, white arrow). The collagen became thicker and darker, inferring that some ACP nanoparticles penetrated the collagen (Fig.5 e, white arrow). After 72 hrs incubation, almost all of the nanoparticles detected on the surface of the remineralized dentin were rod-like in shape (Fig.5 i, black arrow). At 96 hrs, the demineralized dentin was fully remineralized and fused with the surface crystals of the dentin (Fig.5 i). A needle-like HAp layer was found attached to the dentin surface (Fig.5 l, black arrow). Therefore, it can be inferred that some of the ACP nanoparticles on the surface of the remineralized dentin transformed into a needle-like HAp layer with a thickness of 0.2 μm, and some of the ACP nanoparticles migrated through the demineralized layer and entered the collagen to promote intrafiber mineralization of the demineralized dentin.

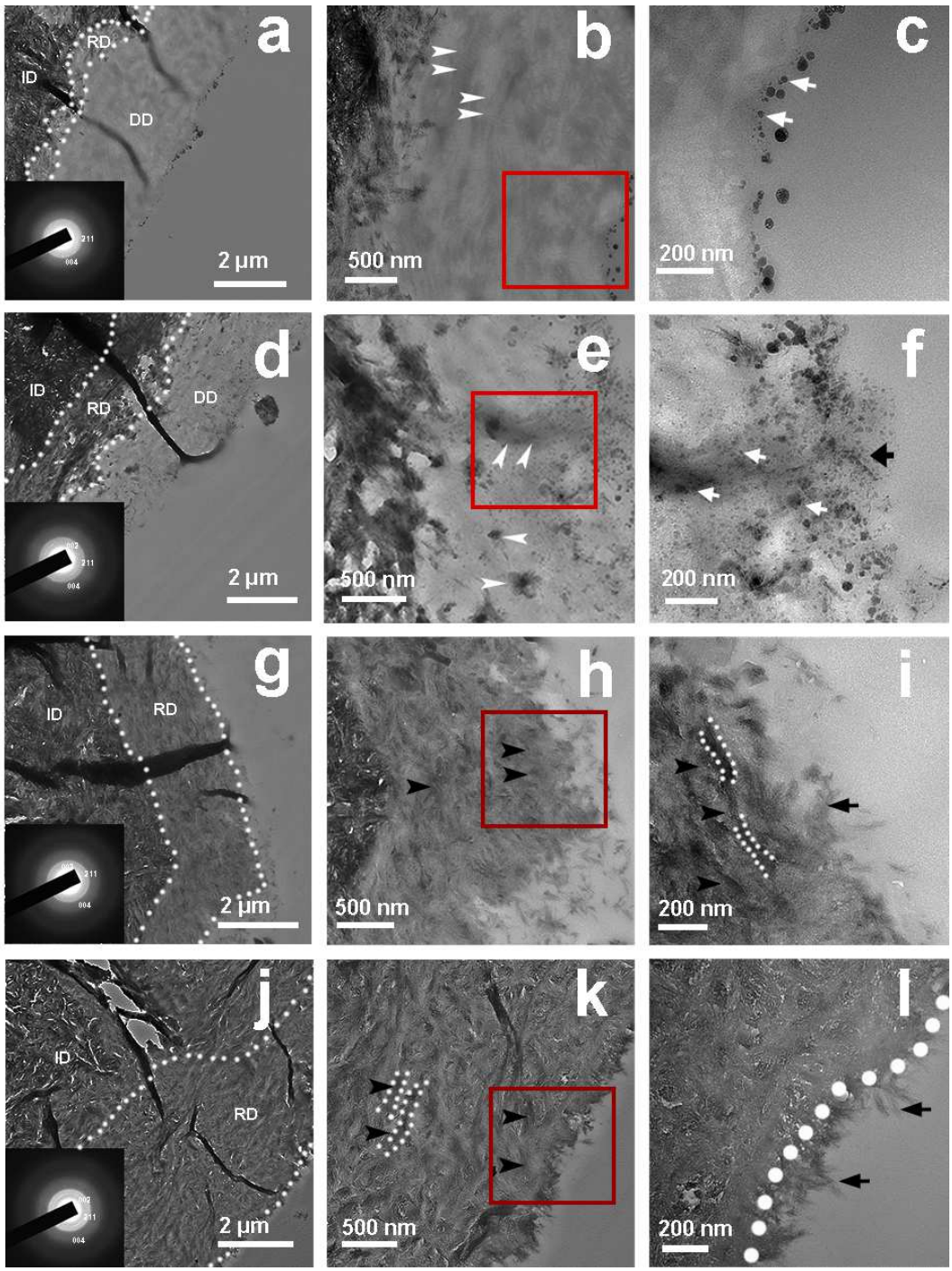

Fig.5 TEM images of dentin treated with the mineralizing film for 24 hrs (panels a-c), 48 hrs (panels d-f), 72 hrs (panels g-i) and 96 hrs (panels j-l). Panels c, f, i and l are high magnifications of panels b, e, h and k, respectively. At 24 hrs, spherical ACP nanoparticles were attached to the surface (c, white arrow). At 48 hrs, some nanoparticles (f, black arrow) were observed on the

surface, and some were observed in the middle of the demineralized dentin layer (e, f, white arrow). The collagen became thicker and darker (e, white arrow). Rod-like crystals were detected on the surface of the remineralized dentin after 72 hrs (i, black arrow), and the demineralized dentin was fully mineralized and fused with the surface crystals of the dentin. A needle-like HAp layer was detected on the dentin surface at 96 hrs (i, black arrow). Both the black arrow and white dotted line (h, i) indicate the remineralized dentin collagen. ID: Intact dentin. DD: demineralized dentin. RD: remineralized dentin.

High-resolution transmission electron microscopy (HRTEM) images show two interplanar spacings: 0.34 nm and 0.28 nm; these spacings are in agreement with those of the 002 and 211 HAp lattice planes, respectively (Fig.6 a). This is consistent with the findings of previous publications. Elemental maps also indicate that Ca and P are uniformly distributed in the remineralization layer (Fig.6 b-d). The different load forces exerted on the demineralized dentin (16 mN), the remineralized dentin (100 mN) and the intact dentin (120 mN) produced the same dent depth (2500 nm) (Fig.6 e). Furthermore, the hardness (0.68±0.17 GPa) and elastic modulus (15.91±2.84 GPa) of the remineralized dentin were nearly restored to those of the intact dentin (0.89±0.14 GPa and 14.99±2.12 GPa, respectively) (Fig.6 f). Both the remineralized and intact dentin exhibited much higher values than the demineralized dentin (0.14±0.06 GPa and 9.42± 2.07GPa) (Fig.6 f).

In addition, mineralization of the demineralized dentin was not detected in the control groups even after 96 hrs incubation (Fig.S3 and S4). This might be attributed to the absence of ACP nanoparticles in the control groups. The HPMC film alone did not induce the mineralization of dentin.

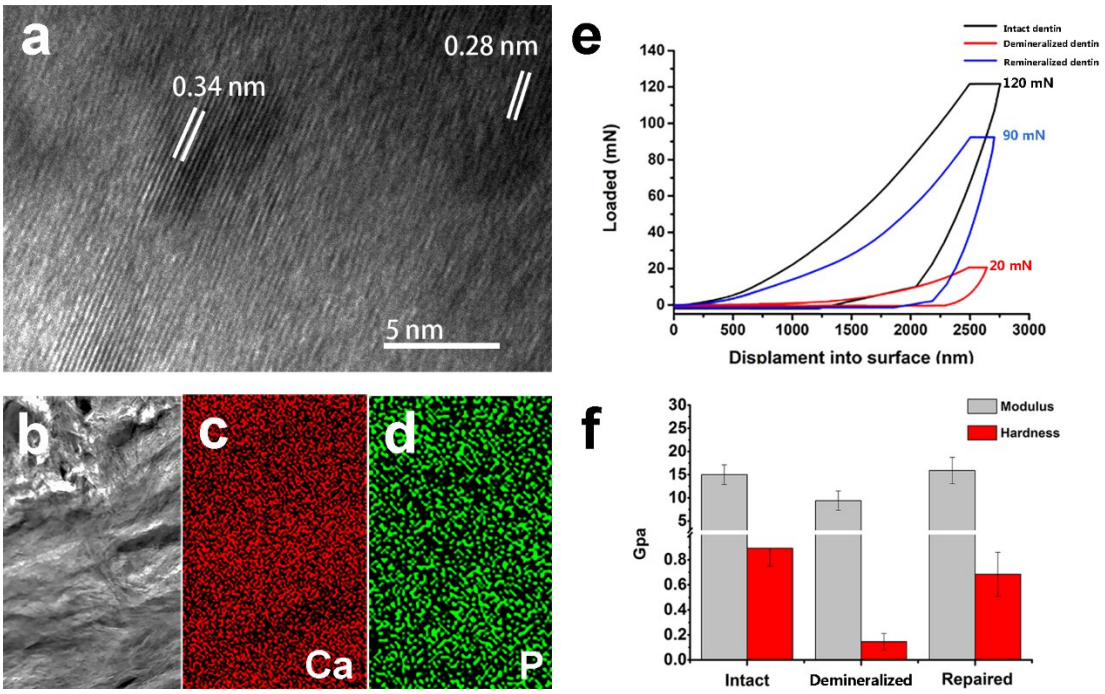

Fig.6 HRTEM images and elemental maps of the demineralized and remineralized dentin; nanoindentation tests on the intact dentin, demineralized dentin and remineralized dentin, in which the demineralized dentin was remineralized for 96 hrs. a: HRTEM image showing the two interplanar spacings, 0.34 nm and 0.28 nm, for the remineralized dentin (panel b). Elemental maps revealing the uniform distribution of calcium and phosphate (panels c, d) in the boxed region (panel b). e: Load-displacement curves showing that the same dent depth (2500 nm) was obtained with the different load forces exerted on the intact dentin (120 mN), demineralized dentin (20 mN) and remineralized dentin (90 mN). f: Hardness and elastic modulus values for the intact dentin, demineralized dentin and remineralized dentin. The mean hardness values for the intact dentin, demineralized dentin and remineralized dentin are 0.89±0.14 GPa, 0.14±0.06GPa and 0.68±0.17 GPa, respectively. The mean modulus values for the intact dentin, demineralized dentin and remineralized dentin are 14.99±2.12 GPa, 9.42± 2.07 GPa and 15.91±2.84, respectively.

In vivo experiments of biomimetic mineralization of dentin

The mineralizing film was used in vivo to promote the remineralization of demineralized dentin in rabbits (Fig.7 a-c). This treatment induced a remineralization layer of approximately 0.6 μm at the bottom of the demineralized dentin after 7 d (Fig.7 d-f). However, remineralization of the demineralized dentin in the rabbits of the control group (treatment with an HPMC film alone) was not detected after 7 d (Fig.S5). The results of the in vivo and in vitro studies are consistent.

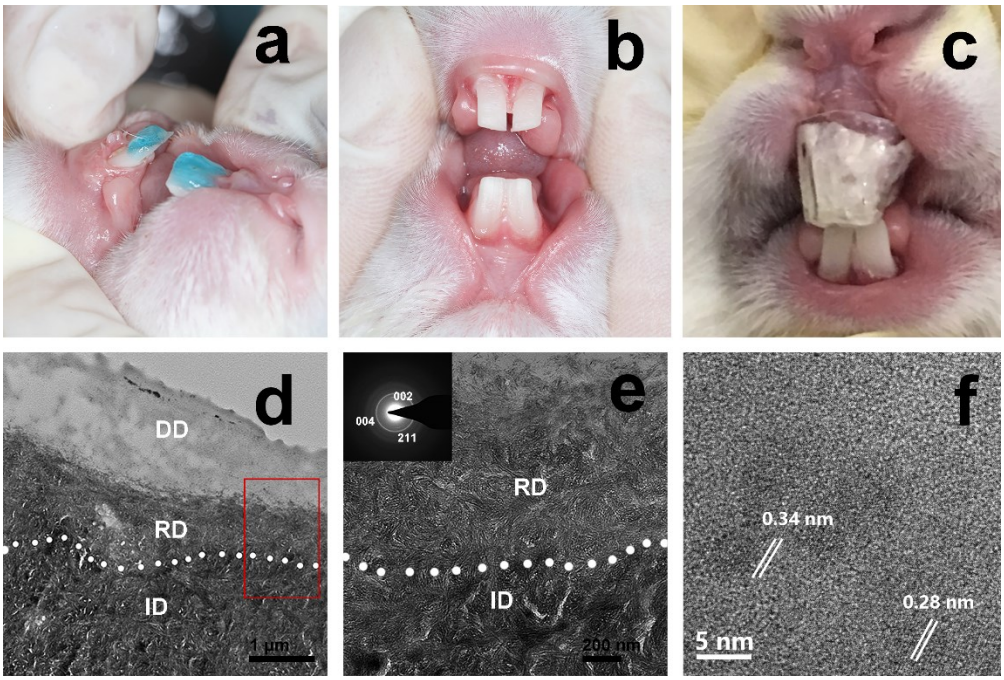

Fig.7 In vivo remineralization of demineralized dentin in rabbits (panels a-c), TEM images of dentin treated with the mineralizing film for 7 d (panels d-f). Panel b shows a magnified view of panel a. The TEM images show that the remineralized layer on the intact dentin was approximately 600 nm thick (panel a). The SAED patterns (insets in panel b) reveal 002, 004, and 211 diffraction rings. The HRTEM image shows two interplanar spacings: 0.34 nm and 0.28 nm. ID: Intact dentin. DD: demineralized dentin. RD: remineralized dentin.

Discussion on the biomimetic mineralization of dentin

The mineralizing film could be used as a novel film to promote the biomimetic mineralization of dentin. HPMC becomes a gel when in contact with water because its polymer chains gradually relax and its volume simultaneously expands [37]. This results in the release of incorporated particles. Moreover, HPMC contains hydrophobic microregions associated with its hydrophobic methoxy groups and promotes the diffusion of loaded particles when in contact with water [17,18]. It has been reported that the hydrophobic microregions are considered physical crosslinking points that integrate the entire gel network [30]. Polymer molecules have a relatively regular arrangement in gels; they do not form in random coils such as that observed in solution. They can provide a certain microenvironment for delivering amorphous precursors and controlling the diffusion of ions in gels [31,37]. The polyhydroxy groups in the hydrophobic microregions can restrain ions and influence the diffusion speed of loaded particles [38]. In this study, when HPMC was in contact with artificial saliva, the PAsp-stabilized ACP nanoparticles diffused into the HPMC gel scaffold (Fig.1 e, f) and were continuously released from the mineralizing film (Fig.2 a). These nanoparticles could act as precursors in the biomimetic mineralization of dentin collagen (Fig. 5 and 7). The FTIR spectra indicated that pure ACP nanoparticles in artificial saliva transformed into HAp within 30 min. When the pure ACP nanoparticles were dispersed in the HPMC matrix, the ACP nanoparticle phase transformation could be slowed to 30-60 min. When the PAsp-stabilized ACP nanoparticles were dissolved in artificial saliva, they began to transform after 2 to 4 hrs. However, when the PAsp-stabilized ACP nanoparticles were fixed in the HPMC matrix, they remained amorphous for over 6 hrs (Fig.S6). PAsp has been recognized as a potent ACP nanoparticle stabilizer due to the chelation of abundant carboxyl groups with calcium ions. The absorption peak corresponding to PAsp-ACP nanoparticle hydroxyl groups changed from 3292 cm^{-1} to 3402 cm^{-1}, indicating that chelation occurred between the carboxyl groups and calcium ions [28]. The broad band at 3460 cm^{-1} observed in the pure HPMC film shifted to 3480 cm^{-1} in the PAsp-ACP-HPMC film, suggesting that there was some interaction between calcium ions and the hydroxyl groups of HPMC. This might account for the increased stabilization of PAsp-ACP in the HPMC film. The synthesis of $CaCO_3$ crystals can be achieved using hydroxypropylmethyl cellulose hydrogels as templates [30]. This infers that HPMC might play a synergistic role in

stabilizing PAsp-ACP precursors for the biomimetic mineralization of dentin (Fig.S7), as HPMC can extend the PAsp-ACP nanoparticle stabilization time in artificial saliva.

In summary, the dentin remineralization process observed in this study can be described as follows. After the mineralizing film attached to the surface of the demineralized dentin, it became gelatinous in artificial saliva, a large number of spherical ACP nanoparticles were rapidly released from the ACP-HPMC film (Fig.5 c white arrow). Then, the spherical ACP nanoparticles penetrated the demineralized layer (Fig.5 e, white arrow). They surrounded the demineralized collagen fibrils (Fig.7 e, f), gradually penetrated the collagen, and transformed into HAp, a process that was mediated by PAsp and HPMC. Finally, the demineralized dentin was heavily remineralized (Fig.5 i, k, black arrow and white dotted line); this was observed in vitro and in vivo (Fig. 5 and 7). This results of this study may lay the foundation for a novel mineralization strategy in preventive dentistry.

Conclusion

HPMC films can be used as novel amorphous precursor carriers to promote biomimetic mineralization. The novel mineralizing films with excellent biocompatibility might pave the way in the design and fabrication of anti-carious materials for preventive dentistry.

Supplementary Information

The online version contains supplementary material available at ……

Supplementary material: **supplementary text, section 1:** The preparation of demineralized dentin disks, dentin samples for TEM, NFM samples for Cryo-TEM, dentin samples for nanoindentation; The preparation of buccal mucosa samples for microscopic histological observations; The preparation of transparent custom trays; **supplementary text, section 2: tables and figures: Table 1.** Grading system for oral and penile reactions. **Table 2.** Grading system for microscopic examination for oral, penile, rectal and vaginal tissue reaction**. Fig. S1.** the splitting function (SF)

of PAsp-ACP nanoparticles and the novel mineralizing film. **Fig. S2.** The results of the histologic examination. **Fig. S3.** TEM images of demineralized dentin (control group). **Fig. S4.** TEM images of demineralized dentin treated with HPMC film (control group). **Fig. S5.** TEM images of the demineralized dentin of rabbits treated with mineralizing film (control group). **Fig. S6.** FTIR spectra of ACP in different systems. **Fig. S7.** FTIR spectra of pure PAsp, PAsp-ACP, the pure HPMC film the HPMC-PAsp-ACP film, a HPMC-$CaCl_2$ film and a HPMC- Na_2HPO_4 film.

Acknowledgement

We thank Ying Xu, Wei Yin and Mr Xiaokun Ding and Rong Nianhang for their assistance with experiments and characterization studies. Wang Zhe and Zhou Zihuai contributed equally to this work.

Authors' contributions

Z W and BP F designed experiments. Z W and ZH Z. analyzed and interpreted the electrochemical data and wrote the original manuscript. RK T and BP F conducted the experiments. ZY Z, HY Z, ZL Z, JY F, ZH Z performed the data curation, All authors read and approved the final manuscript.

Funding

This work was supported by the National Natural Science Foundation of China (No. 82001097, 81970982) and the Natural Science Foundation of Zhejiang Province, China (No. 2020C03037; No. LQ20H140005).

Availability of data and materials

The datasets used and/or analyzed during the current study are available from the corresponding author upon reasonable request.

Declaration

The authors declare that they have no competing interests.

Consent for publication

All authors agree to be published.

Competing interests

The authors declare that they have no competing interests.

Author details

1 The Affiliated Hospital of Stomatology, School of Stomatology, Zhejiang University School of Medicine, and Key Laboratory of Oral Biomedical Research of Zhejiang Province, Hangzhou, Zhejiang, 310006, China

2 Department of Chemistry, Zhejiang University, Hangzhou, Zhejiang, 310027, China

* Corresponding author:

Baiping Fu, The Affiliated Hospital of Stomatology, School of Stomatology, Zhejiang University School of Medicine, and Key Laboratory of Oral Biomedical Research of Zhejiang Province, Hangzhou, Zhejiang, 310006, China

Tel.: 057187217225; E-mail: fbp@zju.edu.cn.

References

1. Peres, M. A.; Macpherson, L. M. D.; Weyant, R. J.; Daly, B.; Venturelli, R.; Mathur, M. R.; Listl, S.; Celeste, R. K.; Guarnizo-Herreño, C. C.; Kearns, C.; Benzian, H.; Allison, P.; Watt, R. G. Lancet 2019, 394 (10194), 249-260.
2. Bernabé, E.; Marcenes, W. Br. Dent. J. 2020, 229 (7), 487-491.
3. Merchan, M. T.; Ismail, A. I., Measurement and Distribution of Dental Caries. 2021, 154-170.
4. Arifa, M. K.; Ephraim, R.; Rajamani, T. Int J Clin Pediatr Dent 2019, 12 (2), 139-144.
5. He, G.; Dahl, T.; Veis, A.; George, A. Nat Mater 2003, 2 (8), 552-8.
6. Bleek, K.; Taubert, A. Acta Biomater. 2013, 9 (5), 6283-6321.
7. De Yoreo, J. J.; Gilbert, P. U.; Sommerdijk, N. A.; Penn, R. L.; Whitelam, S.; Joester, D.; Zhang, H.; Rimer, J. D.; Navrotsky, A.; Banfield, J. F.; Wallace, A. F.; Michel, F. M.; Meldrum, F. C.; Colfen, H.; Dove, P. M. Science 2015, 349 (6247), 6760.
8. Combes, C.; Rey, C. Acta Biomater. 2010, 6 (9), 3362-3378.
9. Antiope; Lotsari; Anand, K.; Rajasekharan; Mats; Halvarsson; Martin; Andersson. Nat Commun 2018, 9(1),4170-4181.
10. Ms, A.; Shb, B.; Atjvh, B.; Hjh, A.; Ps, B.; Ht, A. Acta Biomater. 2019, 90, 132-145;
11. Wu, D.; Yang, J.; Li, J.; Chen, L.; Tang, B.; Chen, X.; Wu, W.; Li, J. Biomaterials 2013, 34 (21), 5036-5047.
12. Yao, S.; Jin, B.; Liu, Z.; Shao, C.; Zhao, R.; Wang, X.; Tang, R. Adv. Mater. 2017, 29 (14).
13. Al-Dulaijan, Y. A.; Weir, M.; Melo, M.; Sun, J.; Oates, T. W.; Zhang, K.; Xu, H. Dent. Mater. 2018, 34 (12), 1735-1747.
14. Luo, X. J.; Yang, H. Y.; Niu, L. N.; Mao, J.; Huang, C.; Pashley, D. H.; Tay, F. R. Acta Biomater. 2016, 31, 378-387.
15. Wu, Z.; Wang, X.; Wang, Z.; Shao, C.; Jin, X.; Zhang, L.; Pan, H.; Tang, R.; Fu, B. ACS Appl Mater Interfaces 2017, 9 (21), 17710-17717;

16. Wang, Z.; Ouyang, Y.; Wu, Z.; Zhang, L.; Shao, C.; Fan, J.; Zhang, L.; Shi, Y.; Zhou, Z.; Pan, H.; Tang, R.; Fu, B. Nanoscale 2018, 10 (40), 18980-18987.
17. Siepmann, J.; Peppas, N. A. Adv. Drug Del. Rev. 2012, 64, 163-174.
18. Ohara, T.; Kitamura, S.; Kitagawa, T.; Terada, K. Int. J. Pharm. 2005, 302 (1-2), 95-102.
19. Sun, J.; Chen, C.; Pan, H.; Chen, Y.; Mao, C.; Wang, W.; Tang, R.; Gu, X. J. Mat. Chem. B 2014, 2 (28), 4544.
20. Termine, J. D.; Posner, A. S. Nature 1966, 211 (5046), 268-270.
21. Biological evaluation of medical devices. US-ANSI: 2010; Vol. ANSI/AAMI 10993-10-2010.
22. Qi, C.; Zhu, Y. J.; Zhao, X. Y.; Lu, B. Q.; Tang, Q. L.; Zhao, J.; Chen, F. Chemistry - A Euro J 2013, 19 (3), 981-987.
23. Zhou, Z.; Zhang, L.; Li, J.; Shi, Y.; Fu, B. Nanoscale 2021, 13,953-967.
24. Mei, I. B.; Kontrec, J.; Jura In, D. D.; Selmani, A.; D Akula, B. N.; Maltar-Strme Ki, N.; Lyons, D. M.; Plodinec, M.; Ceh, M.; Gajovi, A. Crystengcomm 2018, 20(1), 35-50.
25. Combes, C.; Rey, C. Acta Biomater. 2010, 6 (9), 3362-78.
26. Ding, C.; Zhang, M.; Li, G. Carbohydr. Polym. 2015, 119, 194-201.
27. Kunneng; Liang; Suping; Wang; Siying; Tao; Shimeng; Xiao; Han; Zhou. Int J Oral Sci 2019, 11 (3), 24-35.
28. He, H.; Shao, C.; Mu, Z.; Mao, C.; Gu, X. Carbohydr. Polym. 2020, 2(229), 115547.
29. Xue, Z.; Xue, N. OALib 2020, 07 (4), 1-9.
30. Zhao, J.; Li, Y.; Cheng, G. Chin. Sci. Bull. 2007, 52 (13), 1796-1801.30
31. Khanum, H.; Ullah, K.; Murtaza, G.; Khan, S. A. Int. J. Biol. Macromol. 2018, 120 (Pt B), 1624-1631.
32. Hirshkowitz, M.; Whiton, K.; Albert, S. M.; Alessi, C.; Bruni, O.; DonCarlos, L.; Hazen, N.; Herman, J.; Katz, E. S.; Kheirandish-Gozal, L.; Neubauer, D. N.; O'Donnell, A. E.; Ohayon, M.; Peever, J.; Rawding, R.; Sachdeva, R. C.; Setters, B.; Vitiello, M. V.; Ware, J. C.; Adams Hillard, P. J. Sleep health 2015, 1 (1), 40-43.
33. Tovani, C. B.; Oliveira, T. M.; Soares, M.; Nassif, N.; Ramos, A. P. ACS Appl Mater Interfaces 2020, 12(39), 43422 – 43434.
34. Mokabber, T.; Cao, H. T.; Norouzi, N.; Rijn, P. V.; Pei, Y. ACS Appl Mater Interfaces 2020, 12(5), 5531 – 5541.
35. Ms, A.; Kn, A.; Tt, A.; Yk, B.; Ki, A.; Tk, A.; Ksa, C.; Ynd, E.; Hm, B. J. Photochem. Photobiol. B: Biol. 2019, 201, 111633.
36. Tl, A.; Qb, A.; Jie, S. A.; Rvl, B.; Djb, A. Int. J. Pharm. 2020, 580, 119238.
37. Raucci, M. G.; Giugliano, D.; Longo, A.; Zeppetelli, S.; Carotenuto, G.; Ambrosio, L. J. Tissue Eng. Regen. Med. 2017, 11 (8), 2204-2216.
38. Yang, T.; He, R.; Omeoga, U.; Wang, L.; Sun, R.; Zhang, N.; Wang, W.; Xu, D.; Zeng, D. J. Cryst. Growth 2019, 508, 72-81.
39. Reis, N. M.; Liu, Z. K.; Reis, C. M.; Mackley, M. R. Cryst Growth Des 2014, 14 (7), 3191-3198.

Figure captions:

Fig.1 Characterization of the PAsp-ACP nanoparticles and the novel mineralizing film.

Fig.2 Ca and P release and phase transformations of the novel mineralizing film.

Fig.3 Cryo-TEM images of the novel mineralizing film and its SAED pattern.

Fig.4 Cytotoxicity and oral mucosa irritation tests of the novel mineralizing film.

Fig.5 TEM images of dentin treated with the novel mineralizing film.

Fig.6 HRTEM images and elemental maps of the demineralized and remineralized dentin

Fig.7 In vivo remineralization of demineralized dentin in rabbits and TEM images of dentin treated with the novel mineralizing film for 7 d.

Fig. 1.

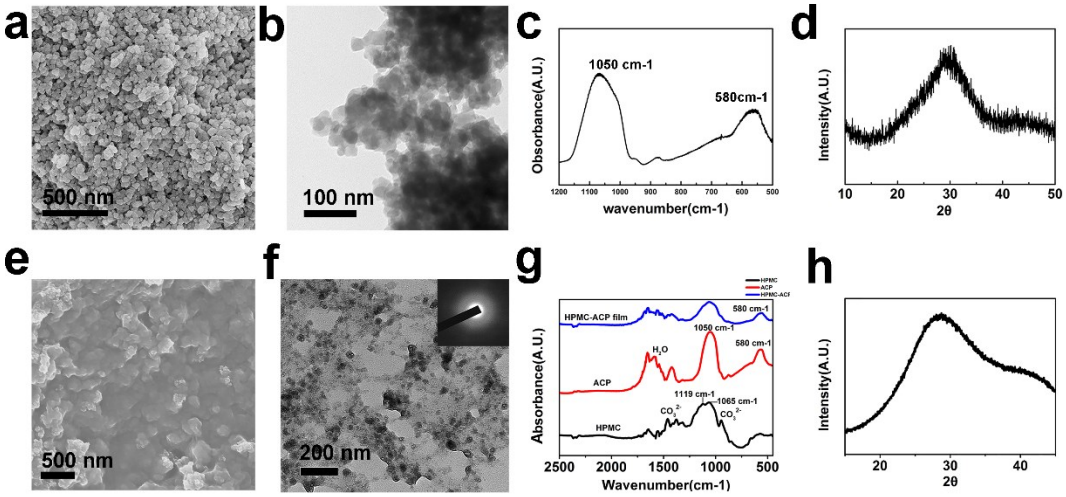

Fig.2

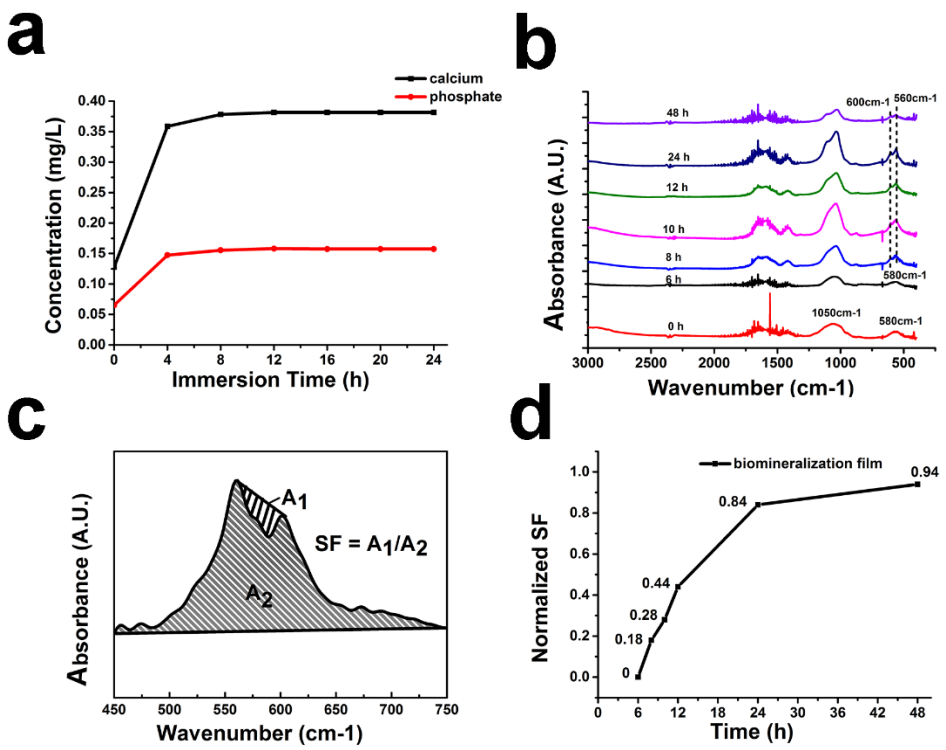
a
calcium
phosphate
Concentration (mg/L)
Immersion Time (h)
b
48 h
24 h
12 h
10 h
8 h
6 h
0 h
600cm-1
560cm-1
580cm-1
1050cm-1
580cm-1
Absorbance (A.U.)
Wavenumber (cm-1)
c
A1
A2
SF = A1/A2
Absorbance (A.U.)
Wavenumber (cm-1)
d
biomineralization film
0.94
0.84
0.44
0.28
0.18
0
Normalized SF
Time (h)

Fig.3

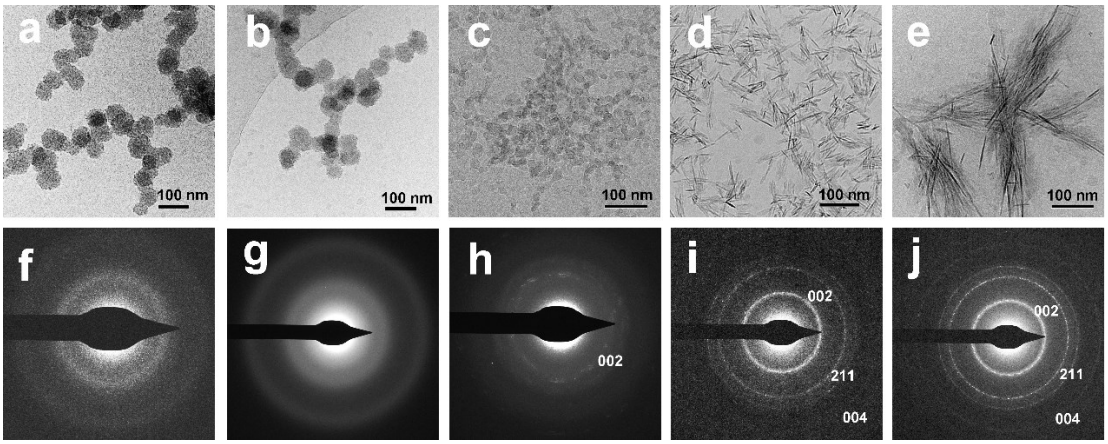
a
b
c
d
e
100 nm
f
g
h
i
j
002
211
004

Fig.4

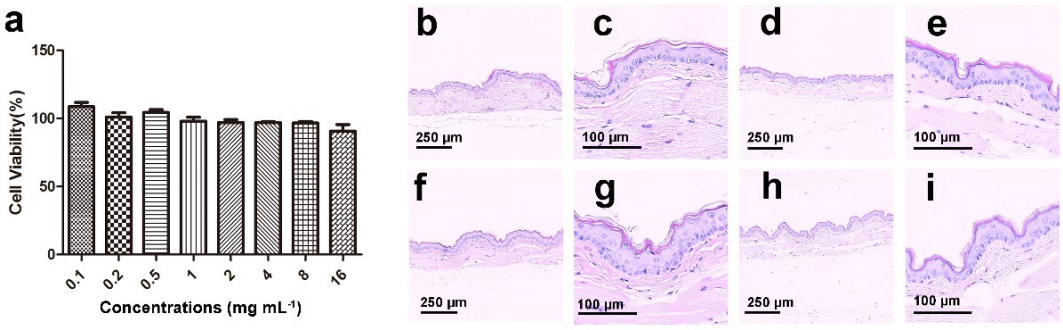
a
150
100
50
0
Cell Viability(%)
0.1
0.2
0.5
1
2
4
8
16
Concentrations (mg mL-1)
b
250 μm
c
100 μm
d
250 μm
e
100 μm
f
250 μm
g
100 μm
h
250 μm
i
100 μm

Fig.5

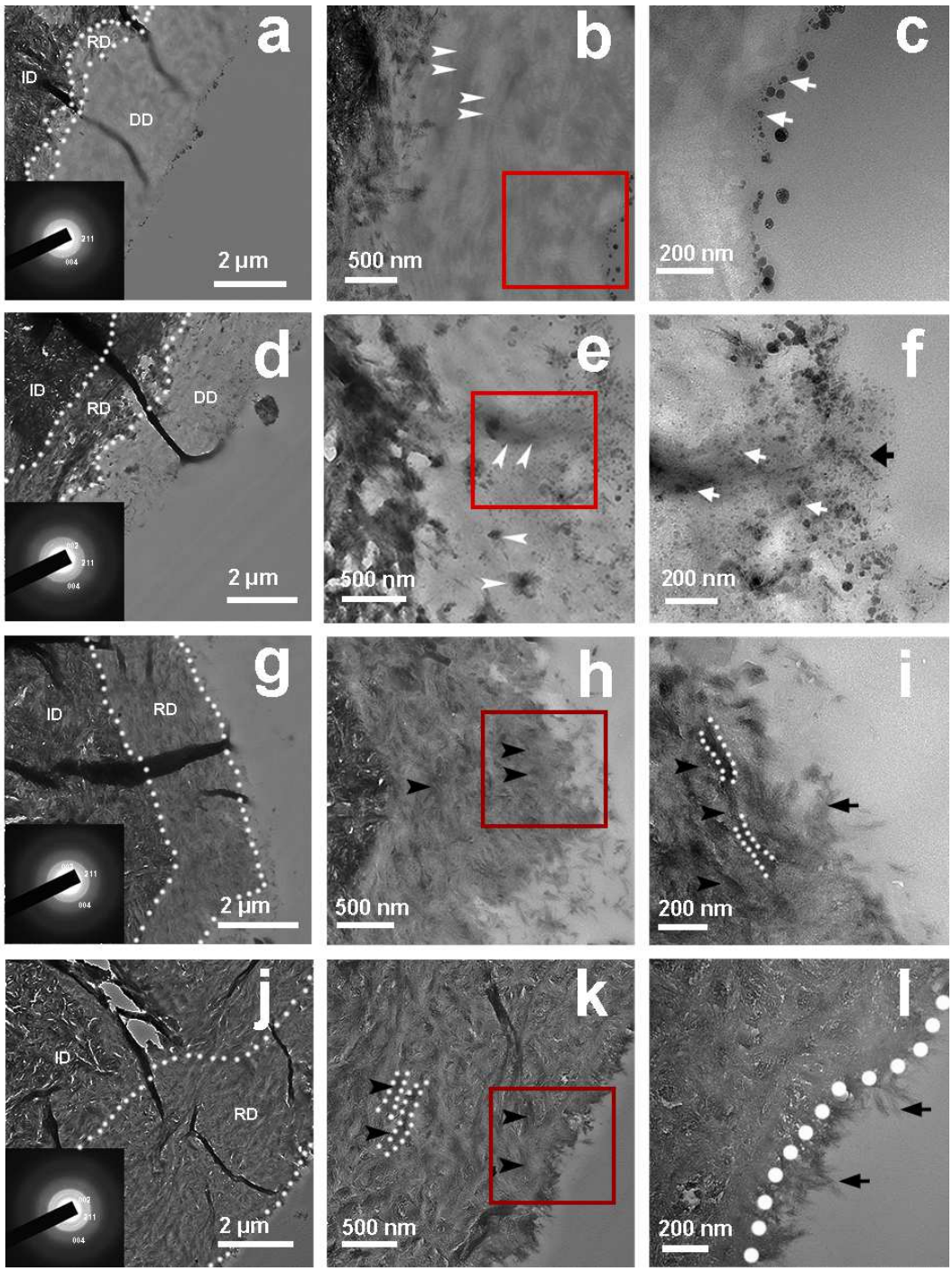
a
RD
ID
DD
2 μm
b
500 nm
c
200 nm
d
ID
RD
DD
2 μm
e
500 nm
f
200 nm
g
ID
RD
2 μm
h
500 nm
i
200 nm
j
ID
RD
2 μm
k
500 nm
l
200 nm

Fig.6

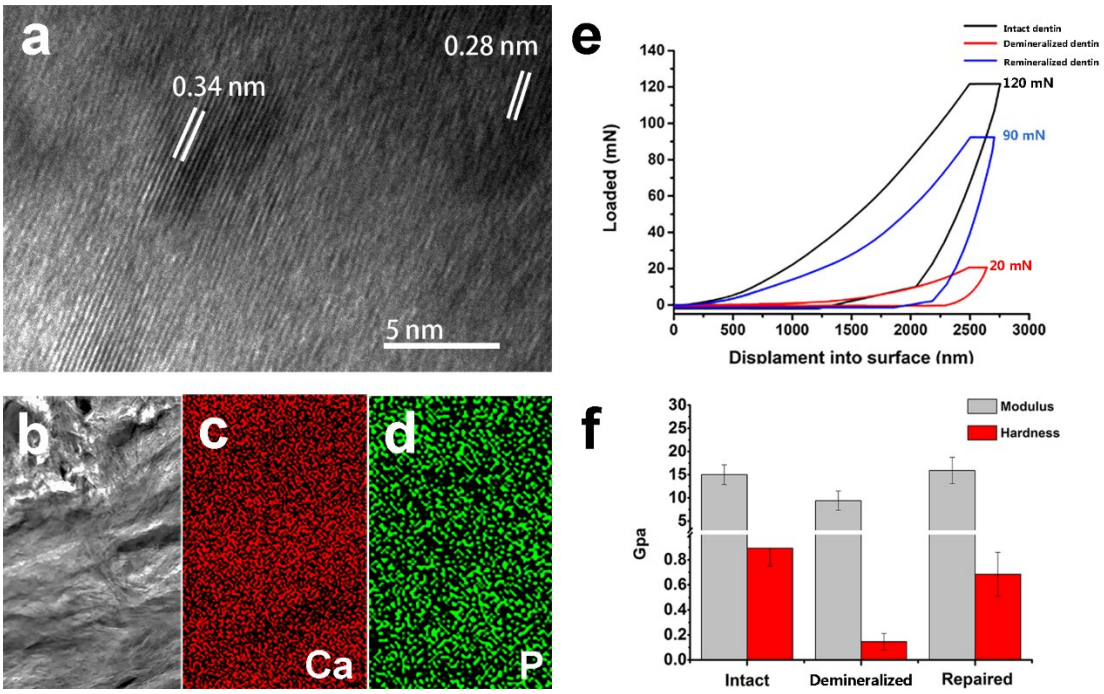
a
0.34 nm
0.28 nm
5 nm
b
c
Ca
d
P
e
Intact dentin
Demineralized dentin
Remineralized dentin
120 mN
90 mN
20 mN
Loaded (mN)
Displament into surface (nm)
f
Modulus
Hardness
Gpa
Intact
Demineralized
Repaired

Fig.7

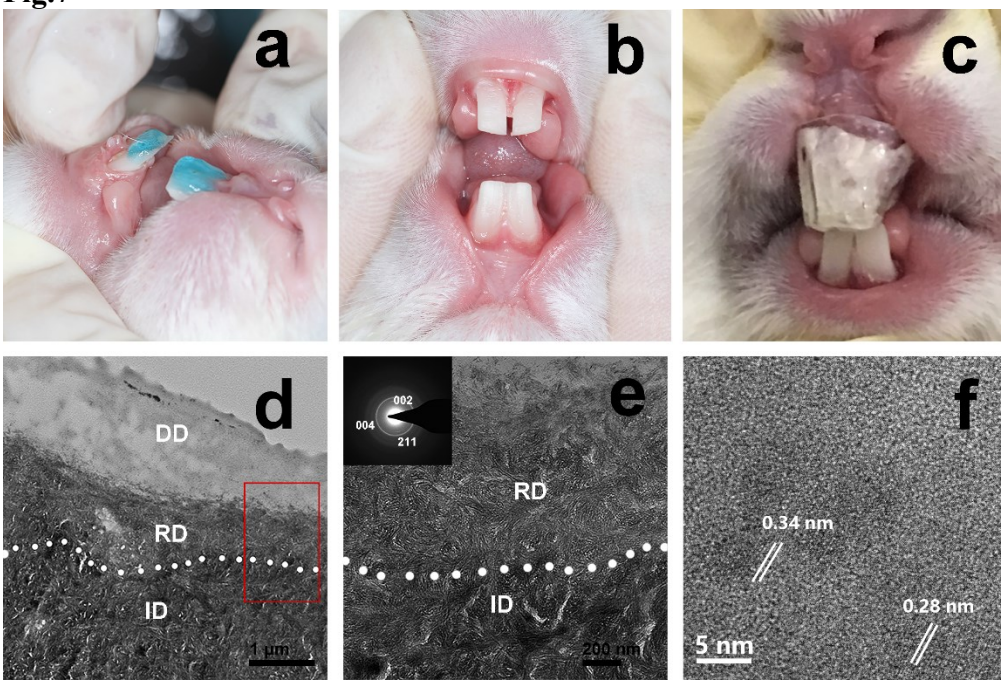
a
b
c
d
DD
RD
ID
1 μm
e
002
004
211
RD
ID
200 nm
f
0.34 nm
0.28 nm
5 nm

Supplementary Files

This is a list of supplementary files associated with this preprint. Click to download.

- renamede0804.tif
- SupportingInformation.docx